Significant Northward Jump of the Western Pacific Subtropical High: the Interannual Variability and Mechanisms

YaNing Wang*, HaiBo Hu*,#, Xuejuan Ren*, Xiu-Qun Yang*, Kefeng Mao[2]

* CMA-NJU Joint Laboratory for Climate Prediction Studies, Instituted for Climate and Global Change Research, School of Atmospheric Science, Nanjing University, Nanjing 210093, China

[2]National University of Defense Technology.

#Corresponding author: H.-B. Hu (huhaibo@nju.edu.cn)

Key Points:

- The anomalous early and late years of the western Pacific subtropical high (WPSH) significant northward jump events in 42 years are revealed.
- In the early years, the tropical geopotential height anomalies in the mid-lower levels determine the time of the WPSH northward jump.
- The upper wave train in the mid-high latitudes and local air-sea interaction control the WPSH northward jump collaboratively in late years.

Abstract

The intensity and position of the western Pacific subtropical high (WPSH) have crucial effects on climate and disaster events in East Asia during summer. The WPSH significant northward jump (SNJ) events are the main manifestation of the seasonal evolution of WPSH, which are important for the precipitation over East Asia. Using the daily reanalysis datasets from year 1979 to 2020, this study further defines the early and late SNJ events of WPSH on the interannual timescale, which are connected separately with the tropical, mid-latitude subseasonal signals and the local air-sea interaction. However, the mechanisms of the WPSH-SNJ events are different in the anomalous early and late years. In the early SNJ years, the subseasonal signals from the mid-level East Asia-Pacific teleconnection pattern or the low-level boreal summer intraseasonal oscillation cause the positive 500 hPa geopotential height anomalies, which contribute to the significant WPSH northward jump in the first pentad of July. However, the above factors are unable to cause the WPSH-SNJ in the late years. Until the second pentad of August, the collaborative effects between mid-high latitudes wave trains over high levels and cold SST anomalies in the core region lead to the barotropic geopotential height anomalies and the lagged northward jump of WPSH.

Key words: western Pacific subtropical high; East Asia-Pacific teleconnection; boreal summer intraseasonal oscillation; upper-level wave train; local air-sea interaction

Plain language summary

The West Pacific Subtropical high (WPSH) is an important component of the East Asian summer monsoon circulation system. The subseasonal northward movement of the WPSH during summer is closely related to the climate of East Asia. However, there are few studies on the interannual variability and the mechanism of the WPSH significant northward jump (SNJ). Focusing on the SNJ events of WPSH, it is found that the time of WPSH-SNJ exhibits significant interannual variability. After selecting the anomalous early and late northward jump years based on the interannual variability, different mechanisms are revealed. The subseasonal signals in the mid-lower levels play a vital role in the WPSH-SNJ in the early years: the circulation anomalies caused by the East Asia/Pacific (EAP) teleconnection pattern or the boreal summer intraseasonal oscillation (BSISO) can affect the meridional position of WPSH and lead to the WPSH-SNJ. However, the EAP and BSISO signals are ineffective in the late years. The WPSH-SNJ events are jointly influenced by the upper wave train and the local air-sea interaction. This study will be helpful to understand the process of the northward jump of the WPSH and to improve the skills of subseasonal climate forecasting in East Asia during summer.

1 Introduction

The Western Pacific Subtropical High (WPSH) is a large–scale anticyclonic circulation system in the mid-lower troposphere over the North Pacific during summer (Huang, 1963; Tao and Chen, 1987). As an important component of the East Asian summer monsoon (EASM) circulation system, the WPSH has a crucial influence on the East Asian summer climate (Ding, 1992; Chang et al., 2000b; Ding and Chan, 2005; Zhou and Yu, 2005). Multiple variabilities of WPSH with different timescales (such as subseasonal, interannual, and interdecadal variabilities) were found (Zhou et al.,2009; He et al.,2015. Chang et al., 2000; Yang and Sun, 2003). To characterize the variations in the intensity and position of the WPSH, some research results (Liu et al., 2012) defined a series of WPSH indices, including the WPSH area index, intensity index, west extension index, and ridge index. Especially, the ridge index represents the meridional position of the WPSH and has an important indication for precipitation over eastern China during summer (Liu et al., 2019). Previous studies suggested that with the subsolar point moving northward during the boreal summer, the WPSH ridge line has a significant seasonal variability. It is also related to the meridional movement of the rain belt in eastern China (Zhang and Tao, 1999; Wang and Ding, 2008; Liang and Ding, 2012; Chen et al., 2016; He and Liu, 2016). These studies found that the significant northward movement of WPSH in summer corresponds to the beginning or end of "Meiyu" in the Yangtze–Huaihe River (YHR) basin. In addition to the influence on the eastern China rain belt in seasonal evolution, the meridional movement of WPSH also has significant interannual variability, which is closely related to the large-scale drought, flood disasters, and extreme heat wave events in East Asia (Liu et al.,2019; Wang et al. 2016; Ding et al., 2021). However, the interannual variability and main

influencing mechanisms of meridional movement of WPSH are still unclear.

Climatologically, the East Asia/Pacific (EAP) teleconnection pattern (Nitta, 1987; Huang and Sun, 1992; Hirota and Takahashi, 2012) is related to the meridional atmospheric dynamic processes and sea surface temperature anomalies (SSTAs) over the western Pacific (Wang et al., 2000; Yang et al., 2007; Xie et al., 2016; Kosaka and Nakamura, 2010). The EAP pattern exhibits strong subseasonal variability with an oscillation period of 25-60 days (Bueh et al. 2008; Wu et al., 2013; Li et al., 2014). In different phases of the EAP pattern, anomalous anticyclones or cyclones will occur over the YHR basin and Japan, which will cause the meridional displacement of WPSH (Huang et al., 2012). In addition, the tropical intra-seasonal oscillation (ISO) also plays a dominant role in the meridional movement of WPSH on subseasonal timescales (Madden, 1986; Wang and Rui, 1990; Zhang and Dong, 2004; Kikuchi et al., 2012). The tropical ISO mode in the Indo-Pacific warm pool during summer is called boreal summer intraseasonal oscillation (BSISO). It is one of the most prominent sources of short-term climate variability in the Asian summer monsoon region (Wang and Xie, 1997; Lin, 2013; Hsu et al., 2016; Lee et al., 2017). Using multivariate empirical orthogonal function (MV-EOF) analysis, Lee et al. (2013) suggested that the propagation of BSISO has an effect on the subseasonal OLR and geopotential height fields over the western North Pacific (WNP). They also defined two real-time indices: BSISO1 index and BSISO2 index. The BSISO1 represents the northward/northeastward propagation of the boreal summer ISO mode in the Indian Ocean with a quasi-oscillation period of 30-60 days. The BSISO2 indicates the northward/northwestward propagation of ISO mode over the Western Pacific and East Asia, with a period of 10-30 days. The active ISO over the WNP can stimulate a poleward propagating Rossby wave, which is favorable for the northward movement of the WPSH. The accumulated effect of the tropical ISO convections in the meridional displacement of WPSH are also discussed (Huang et al., 2020).

In addition to the above tropical factors, the mid-latitude zonal wave trains are proved to influence the WPSH, such as the silk road wave train (SRP) and circumglobal teleconnection (CGT) wave train (Branstator,2002; Lu et al. 2002; Enomoto et al., 2003; Ding and Wang, 2005; Chen and Huang,2012). As the wave train propagates eastward along the atmospheric westerly jet, the energy of the zonal wave train can transmit to the eastern coast of China by forming a ridge or trough. This process has been proved to influence the zonal movement of the WPSH (Tao and Wei,

et al., 2007; Xie et al., 2009; Zhou et al., 2009; Chung et al., 2011; He and Zhou, 2015). Ren et al. (2013) suggested that the persistent warm SSTAs under the west of the WPSH are conducive to the transformation of low-level anomalous anticyclone into a cyclone. Qian and Shi (2017) noted that the interannual SSTAs over the tropical western Pacific can lead to the zonal position of WPSH showing anomalous response. Guan et al. (2019) further pointed out that the local air-sea interaction plays different roles in different stages of the subseasonal variability of WPSH. During the WPSH westward extension stage, the negative SSTAs covering the East Asian coastal water south of 30°N are favorable for the enhancement of local anomalous anticyclones. During the WPSH eastward retreating stage, the persistent warm SSTAs promote the transition from low-level anomalous anticyclone into a cyclone. However, the relationship between the meridional movement of WPSH and the local SSTAs remains to be clarified.

To sum up, this study will focus on the interannual variability of the significant northward jump events of WPSH during summer, which is defined in section 2. Besides, the following impact factors on the meridional movement of WPSH will be discussed: (1) the northward propagation of subseasonal signals from the tropics mid-lower levels, (2) the east-propagating upper-level wave train at mid-latitudes, (3) the SSTAs over the Western Pacific. The remainder of this study is organized as follows: Section 2 introduces the data, methods, and the definition of significant northward jump events of WPSH during summer. Section 3 investigates the interannual variability and different climatic effects of the WPSH significant northward jump events, which can be selected as early and late northward jump years. Section 4 examines the importance of northward propagation of subseasonal signals in the mid-lower levels for the anomalous early northward jump years. Section 5 reveals the combined forcings by the east-propagating upper-level wave train at mid-latitude and the local SSTAs over the WNP for the anomalous late northward jump years. The summary and discussions are given in Section 6.

2 Data and Methods

In this study, daily gridded observations of precipitation covering global land areas are from the US Climate Prediction Center (CPC) with a spatial resolution of 0.5°×0.5°. The daily mean outgoing longwave radiation (OLR) grid data are from the National Oceanic and Atmospheric Administration (NOAA) with a spatial resolution of 1°×1°. In addition, we use the data for daily atmospheric circulation from the fifth generation ECMWF atmospheric reanalysis dataset of the global climate (ERA-5) with a spatial resolution of 1°×1°. All datasets cover the period 1979–2020.

The composite and correlated analyses of meteorological statistical methods are used, and statistical significance tests are based on the Student's t-test. We use pentad as the time unit. To extract the subseasonal variations, we first remove the daily climatology for all variables and then take a 5-day running mean (Krishnamurthy and Shukla, 2000).

The meridional position of WPSH is represented by the ridge index, which is defined as follows: the averaged latitudes satisfying both u=0 and u/ y 0 conditions in a closed 5880 gpm contour over the area (north of 10° N, 110–150° E). If 5880 gpm contour does not exist, then calculate the averaged latitudes satisfying both u=0 and u/ y 0 conditions in a closed 5840 gpm contour (Liu et al., 2012; Liu et al.,2019).

Fig. 1a displays the climatological 500 hPa geopotential height (Z500), horizontal winds, and precipitation fields during summer, the 5880-gpm isocline at the 500 hPa geopotential height field (5880-line) represents WPSH. It can be observed that the main body of the WPSH zonally extends over the WNP, and the average of the WPSH ridge line is 26°N. The south flank of the WPSH is occupied by tropical easterly flow, and the north flank is subtropical easterly flow. The southwest side of the WPSH is occupied by southeast flow, which delivers warm and wet air from the ocean to the mainland. The abundant rainfall is observed over the area located at the outer edge of the WPSH, such as Southern China, southern Japan, the Korean Peninsula, and the Philippines. However, the position of the WPSH ridge line is not constant. As shown in Fig. 1c, the WPSH ridge line has significant subseasonal variability during the summer. In early June, the WPSH ridge index is 20°N and keeps moving northward. It reaches the summer average latitude of 27°N in the fourth pentad of July, then moves northward rapidly, reaching the maximum summer latitude of 31°N in the first pentad of August. After that, the WPSH ridge line retreats southward. In mid-late August, the WPSH ridge index remains near 29°N. The ridge index pentad increment shows that, before the first pentad of August, the WPSH ridge line keeps moving northward, but the amplitude is different in each pentad. The amplitude in the third pentad of June, the first, fourth, and fifth pentad of July are significant, but in the fourth pentad of July is the largest. In the second pentad of August, the WPSH southward recedes obviously, and then the ridge line occurs meridional oscillation.

In the fourth pentad of July, since the WPSH ridge index exceeds the average summer latitude (27°N) and the north shift amplitude is the largest, we consider the latitude value of 27°N in this pentad as the critical latitude. Based on the critical latitude, we define the significant northward jump (SNJ) event of WPSH: if the ridge index of WPSH exceeds 27°N for the first pentad and the ridge index of the next two pentads is greater than or equal to 27°N, an SNJ event is selected, and the first pentad exceeding 27°N is defined as the WPSH-SNJ time.

The SNJ event has important climatological significance. Fig. 1b depicts the difference between the after and before of the SNJ event, including the precipitation and the 500hPa horizontal wind fields. The 5880-lines are also shown. After the SNJ, the WPSH moves northward from 24°N to 30°N. An anticyclone is evident over the mid-latitude North Pacific, with easterlies near 30°N. Due to the influence of water vapor transport caused by wind field variation, the amount of precipitation increases in Northern China, the Korean Peninsula, and the Indian Peninsula, and decreases in Southern China, the YHR basin, and

southern Japan. Therefore, before and after the WPSH-SNJ, the atmospheric circulation and precipitation fields in East Asia are distinct. The interannual evolution of the WPSH-SNJ time from 1979 to 2020 is shown in Fig. 2. In the next chapter, we will investigate the interannual variability of the WPSH-SNJ time.

Based on the previous studies (Bueh et al. 2008; Kosaka and Nakamura,2010), for EAP pattern, we define the daily EAP index according to its activity center as Equation (1):

(1)

In Equation (1), Z500 represents the standardized daily Z500 anomalies. When the EAP index is positive (EAP positive phase), East Asia and its coastal regions present a "+-+" meridional wave–train pattern from low to high latitude; when the EAP index is negative (EAP negative phase), it shows a "-+-" pattern.

When discussing the influence of BSISO on WPSH, we follow the previous studies (Lee et al., 2013). The MV-EOF analysis conducts on the subseasonal anomalies of daily OLR and 850hPa zonal winds in the East Asian summer monsoon region. BSISO1 consists of the first and second EOF modes, and BSISO2 consists of the third and fourth EOF modes. BSISO1 index and BSISO2 index are calculated as follows:

BSISO1 index= (2)

BSISO2 index= (3)

When the BSISO1/BSISO2 index exceeds 1, this day is defined as a BSISO1/BSISO2 active day.

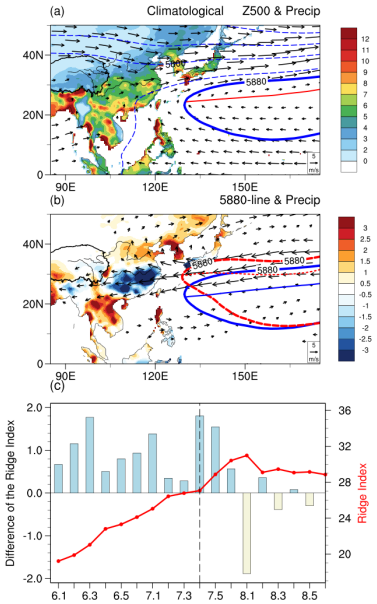

Figure 1. (a) Climatological 500 hPa geopotential height (Z500, contour of 60–gpm intervals), horizontal winds (vector, m s^{-1}), and rainfall (shaded, mm day^{-1}) from 1979–2020. The blue thick contour line and the red line indicate the 5880-line and the WPSH ridge line, respectively. (b) The difference between the after and before of the WPSH-SNJ event, including the precipitation (shaded, mm day^{-1}) and the 500hPa horizontal wind(vector, m s^{-1}) from 1979-2020 during summer. The blue contour line/solid line is the average 5880-line/ridge line before the WPSH-SNJ, and the red contour line/dotted line is the average 5880-line/ridge line after the WPSH-SNJ. (c) Climatological WPSH ridge index (red line, corresponding to the right y-axis) and pentad increments of ridge index (bar, corresponding to the left y-axis) from 1979 to 2020 during summer.

3 The interannual variability of the WPSH-SNJ time

After defining the WPSH-SNJ event, to investigate the interannual variability, Fig. 2 shows the interannual evolution of the WPSH-SNJ time during summer from 1979 to 2020. It is shown that the WPSH-SNJ time has prominent interannual variability. The climatological SNJ time is the fourth pentad of July. The years with WPSH-SNJ time less than one standard deviation of the climatological mean are selected as early years, which are 1981, 1984, 1994, 2001, 2002, 2011, and 2018 (seven years in total). The mean SNJ time of the early years is the fourth pentad of July. The years with WPSH-SNJ time exceeding one standard deviation of the climatological mean are selected as late years, which are 1980, 1983, 1987, 1998, 2003, 2007, 2010, and 2018 (seven years in total). The mean WPSH-SNJ time of the late years is the second pentad of August.

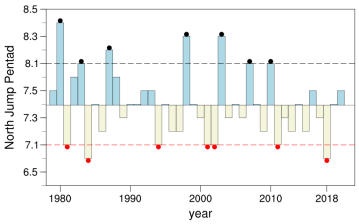

Figure 2. The interannual evolution of WPSH-SNJ time from 1979–2020 (unit: pentad). The yellow and blue bars indicate that WPSH-SNJ time is earlier and later than the climatological mean, respectively. The red and black dots represent the WPSH-SNJ early years and late years, respectively.

To compare the characteristics before and after SNJ for the early and late years respectively, Fig. 3a firstly depicts the difference between the after and before of

the SNJ event in the early years, including the precipitation and the 500hPa horizontal wind fields. The corresponding 5880-line is also shown. Before the SNJ, the WPSH zonally extends over the WNP, and the WPSH ridge line locates around 23°N. After the SNJ, the main body of the WPSH moves northward significantly, and the average position of the ridge line is around 30°N. The intensity of WPSH weakens, and the west extension ridge point retreats eastward. The situation in the late years (Fig. 3b) is different. Before the SNJ, the west extension ridge point of WPSH is westward. After the SNJ, the WPSH maintains stably over the WNP without retreating eastward or weakening, but the amplitude of the north shift is less than that in the early years. After the SNJ, the average of the WPSH ridge line is near 27°N.

The precipitation field of early years (Fig. 3a) shows that, after the SNJ, there is a tripolar precipitation anomaly pattern along the coast of East Asia. The amount of precipitation increases in Northern China, the Korean Peninsula, and the Indian Peninsula but decreases in Southern China, the YHR basin, and southern Japan. This precipitation difference is due to the variation of water vapor transport caused by the wind field. In the late years (Fig. 3b), the same tripolar precipitation anomaly as in the early years occurs. However, compared with the early years, the precipitation variation is different. The precipitation increment in the Korean Peninsula is fewer, while in the Indian peninsula is more significant.

The above discussion indicates that the WPSH-SNJ time has interannual variability. The early and late years have different impacts on rainfall in East Asia. However, what is the influencing factor for the interannual variability of the WPSH-SNJ time? In the following, we will have a discussion.

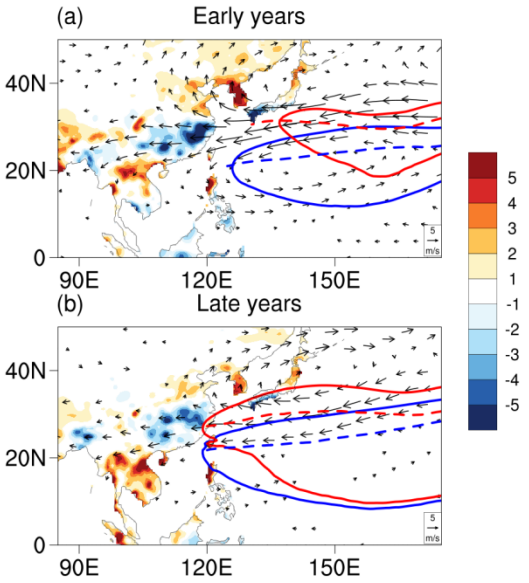

Figure 3. The difference between the after and before of the SNJ event in (a) early years and (b) late years, including the precipitation (shaded, mm day^{-1}) and the 500hPa horizontal winds (vector, m s^{-1}). The blue contour lines/dotted lines are the average 5880-line/ridge line before the WPSH-SNJ, and the red contour lines/dotted lines are the average 5880-line/ridge line after the WPSH-SNJ.

4 The characteristics and mechanisms of the WPSH-SNJ early years

4.1 The anomalous characteristics of the WPSH-SNJ early years

In this chapter, we will focus on the characteristics and possible mechanisms for the early years. Fig. 4 shows the pentad evolution from June 6th pentad - July 3rd pentad (the SNJ pentad and two pentads before and after) for early years, including the and 500 hPa horizontal wind anomalies. Before the SNJ (Fig. 4a), WPSH is zonally elongated over the subtropical western Pacific. The WPSH ridge line is north of the climatological mean, near 25°N. In the sixth pentad of June, the Z500 anomalies presents a "-+-" pattern in the subtropical western Pacific, Japan, and northeast East Asia. The 500 hPa wind anomalies show a "cyclone - anticyclone – cyclone" pattern. This situation is similar to the negative phase of the EAP pattern. During the SNJ pentad (Fig. 4c, the first pentad of July), the positive Z500 anomalies near Japan (the purple box in the middle) further strengthens, which is conducive to the northward migration of WPSH. Meanwhile, the ridge index shifts to 29°N. The rapid Z500 anomalies intensification in the middle purple box plays a vital part in the WPSH-SNJ. Therefore, we define this region (30-40°N, 112.5-137.5°E) as the core region for the early years. After the SNJ (Fig. 4d, e, the second and third pentad of July), WPSH retreats eastward and weakens rapidly.

4.2 The mechanisms of the WPSH-SNJ early years

It can be seen from Fig. 4c that the Z500 anomalies field in the SNJ pentad is similar to the EAP pattern. To explore the relationship between the EAP pattern and the WPSH-SNJ in the early years, Fig. 5 shows the pentad-evolution of the composites WPSH ridge index and EAP index of the early years during summer. The WPSH ridge line of the early year is farther north than the climatological mean (Fig. 1c). In early June, the WPSH ridge index is near 20°N and keeps moving northward. The WPSH keeps moving northward with a large amplitude from mid-June. In the first pentad of July, the WPSH completes the SNJ, with the WPSH ridge index exceeding 28°N. WPSH continues to move northward in the fourth pentad of July. In the sixth pentad of July, WPSH is in the northernmost position (33°N). The WPSH occurs meridional oscillation during August.

As for the evolution of the EAP index, it is negative in the SNJ pentad (the first pentad of July). Meanwhile, the Z500 anomalies field along the East Asian coast shows a "-+-" pattern, which was favorable for the WPSH-SNJ. We also find that the EAP index turns negative one pentad before the SNJ pentad (in the sixth pentad of June). The advanced occurrence and maintenance of the

EAP negative phase are conducive to the positive Z500 anomalies appearing in the core region, which leads to the WPSH-SNJ.

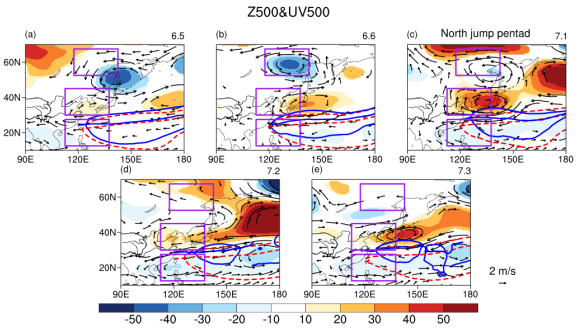

Figure 4. From June 5th pentad - July 3rd pentad for early years, the composite subseasonal anomalies of Z500 (shaded, gpm) and 500hPa horizontal wind (vector, m s^{-1}). The shading areas and vectors are shown only when they are significant at the 95% confidence level. The blue solid contours and red dotted contours represent the 5880-line for early years and the climatological mean, respectively. The blue solid and red dotted lines denote the WPSH ridge line for early years and climatological mean. The purple boxes indicate the three active centers of the EAP pattern.

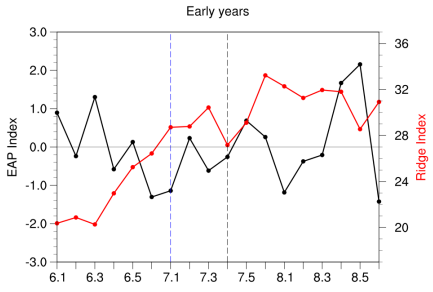

Figure 5. The pentad evolution of EAP index (black line, corresponding to the

left y-axis) and WPSH ridge index (red line, corresponding to the right y-axis) for early years during summer.

It can be concluded from the above that the Z500 anomalies in the core region are very vital for the WPSH-SNJ. Except for the meridional EAP wave train, previous studies indicated that BSISO1 can also influence geopotential height anomalies (Lee et al., 2013; Lin, 2013). Therefore, we will investigate the corresponding relation between BSISO1 and the WPSH-SNJ. Fig. 6a shows the phase space diagram of BSISO1 from June 6th pentad - July 3rd pentad for the early years. Although BSISO1 propagates from phase 1 to phase 8, the distribution in each phase is not uniform. The BSISO1 is very active in Phases 5-6, and their total proportion reaches about 42%. The composite of OLR and 850-hPa wind anomalies of BSISO1 in Phase 1–8 during the same period is also shown (Fig. S1 in the supporting information file). During Phase 5 (Fig. S1e), anomalous convection related to BSISO1 is enhanced over the South China Sea (SCS) and tropical WNP. During Phase 6 (Fig. S1f), the enhanced convection is transmitted to the northwest and strengthened. The active days in Phases 5–6 for early years are also more than the climatological mean (Fig. 6b).

What is the impact of BSISO1 (Phases 5-6) on the WPSH-SNJ? Fig. 6c composites the convection and circulation anomalies fields in Phases 5-6 of BSISO1 from June 6th pentad - July 3rd pentad for early years. As shown in the picture, the enhanced convection is over the SCS and Philippines Islands, with anticyclonic circulation and negative Z500 anomalies over its northwestern part. Suppressed convection is observed over the south of Japan, which affects the positive Z500 anomalies occurring in the core region (purple box). Therefore, the active BSISO1 can influence the circulation anomalies in the core region, which is conducive to the WPSH-SNJ. In addition, our results also show that BSISO2 has a weak influence on the geopotential height anomalies over the core location (Figure omitted).

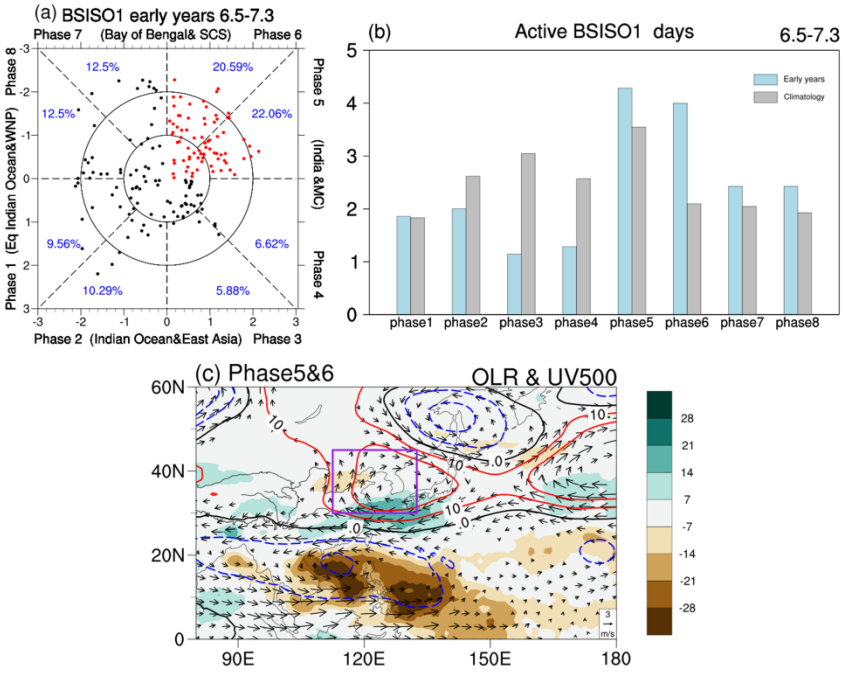

Figure 6. From June 5th pentad - July 3rd pentad for early years, (a) the phase space diagram of BSISO1, the blue words represent the percentage of the days' number in each phase. (b) The active BSISO1 days in phases 1-8 (bar, unit: day), the blue and grey bars represent the active days for early years and the climatological mean, respectively. (c) The composite subseasonal anomalies of OLR (shaded, W m^{-2}), 500hPa wind (vector,m s^{-1}) and Z500 (contour, the solid red lines and dotted blue lines indicate positive and negative value, respectively) of active BSISO1 days in Phase 5–6, the shades and vectors are shown only when they are significant at the 95% confidence level. The purple box indicates the core region of the early years.

For each year in the early years, we obtain Table. 1 according to the pentad-evolution of the EAP index and the phase space diagram of BSISO1. Table. 1 shows the contribution of the EAP pattern and BSISO1 to each year. For some years (1981, 2002), BSISO1 works independently. In other years (1984, 1994, 2001, 2011, 2018), the EAP pattern and BSISO1 all play a role. The specific composite results are shown in Fig. S2, which confirms the conclusion in Table .1. It indicates that the effects of the EAP pattern and BSISO1 in the early years on the WPSH-SNJ are independent.

Early years	1981	1984	1994	2001	2002	2011	2018
EAP	×	√	√	√	×	√	√
BSISO1	√	√	√	√	√	√	√

Table 1. The contributions of EAP pattern and BSISO1 for each early year, where "√" indicates contributions and "×" indicates no contributions.

To sum up, the characteristic of the early years is the "-+-" Z500 anomalies pattern along the East Asian coast during the SNJ pentad. The region (30-40°N, 112.5-137.5°E) is regarded as the core region. The negative phase of EAP pattern and BSISO1 can affect the core region's geopotential height anomalies, which leads to WPSH-SNJ in the early years. What are the characteristics and mechanisms of the late years? We will explore this in the next chapter.

5 The characteristics and mechanisms of the WPSH-SNJ late years

5.1 The anomalous characteristics of the WPSH-SNJ late years

To explore the characteristics of the circulation anomalies in the late years, Fig. 7 shows the pentad-evolution of the Z500 and 500 hPa horizontal wind anomalies, which are from July 6th pentad - August 4th pentad (the SNJ pentad and two pentads before and after). Before the SNJ (Fig. 7a, the sixth pentad of July), the WPSH ridge line is more southern than the climatological mean. The positive Z500 anomalies appear near the subtropical WNP. In the first pentad of August, the WPSH ridge line moves slightly to the north, basically coincident with the climatological mean. A weaker positive Z500 anomalies appear on the north side of the WPSH (the area indicated by the green box). During the SNJ pentad (Fig. 7c, the second pentad of August), the positive Z500 anomalies in the green box further strengthens. As a result, the WPSH ridge line moves further northward, clearly surpassing the climatological mean ridge line. We can conclude that the positive Z500 anomalies in the green box are in favor of the WPSH-SNJ. Therefore, the area shown in the green box (32.5-47.5°N, 147.5-172.5°E) is defined as the core region for late years. After the SNJ (Fig. 7d, e, the third and fourth pentad of August), the WPSH maintains its original position while the positive Z500 anomalies in the core region weaken rapidly.

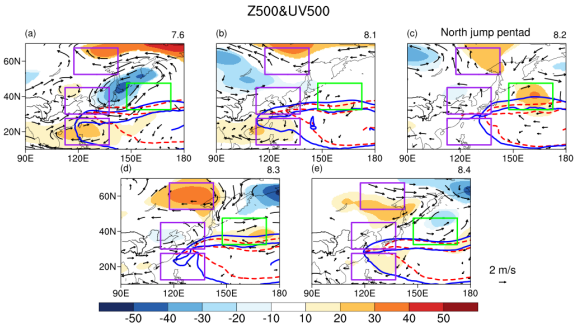

Figure 7. As in **Figure 4** but for the late years from July 6th pentad -August 4rd pentad.

5.2 The mechanisms of the WPSH-SNJ late years

The results in Chapter 4 show that the subseasonal signals in the mid-lower levels play a vital role in the WPSH-SNJ for the early years. In this section, we will explore whether these signals have the same effect on the late years.

To explore the influence of the EAP pattern, Fig. 8 shows the composites pentad-evolution of the WPSH ridge index and EAP index in the late years during summer. The WPSH ridge line in the later years is more southerly throughout the summer. In early June, the WPSH ridge index is near 16°N. and keeps moving northward. After that, the WPSH moves northward continuously with a lesser amplitude. In the fourth pentad of July (the climatological SNJ pentad), the WPSH rapidly moves northward to around 29°N and then retreats to the south in the next pentad. Subsequently, the WPSH continues to move slowly northward. After the second pentad of August (the SNJ pentad), the WPSH ridge index remains near 28°N. The evolution of the EAP index illustrates that, in the sixth pentad of July, the EAP index is positive. Meanwhile, a meridional "+-+" tripolar pattern appears along the East Asian coast, and the negative Z500 anomalies near Japan causes the WPSH to remain in the southern position (Fig. 7c). In the SNJ pentad (the second pentad of August), the negative EAP index is still maintained, which is not conducive to the WPSH-SNJ. Therefore, the EAP pattern does not contribute to the WPSH-SNJ in late years.

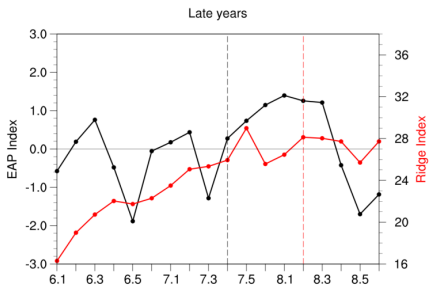

Figure 8. As in Figure 5 but for the late years situation.

Similar to the above, we will investigate the impact of the BSISO1 on WPSH-SNJ in late years. Fig. 9a shows the phase space diagram of BSISO1 from July 6th pentad -August 4th pentad (the SNJ pentad and two pentads before and after) for the late years. The distribution in each phase is not uniform. The BSISO1 is very active in Phases 2-4, and their total proportion is about 51%. During Phases 2-4, anomalous convection related to BSISO1 is enhanced over the Bay of Bengal, Maritime Continent, and SCS (Fig. S3). The active days in Phases 2–4 for late years are also more than the climatological mean (Fig. 9b).

Fig. 9c composites the convection and circulation anomalies fields in Phases 2–4 of BSISO1 from July 6th pentad -August 4th pentad for late years. As shown in the picture, the suppressed convection is observed over the SCS and the tropical WNP, with a large-scale anticyclonic circulation and positive Z500 anomalies over its northwestern part. Enhanced convection is over Japan island, which affects the weak negative Z500 anomalies occurring in the core region (purple box). Therefore, the circulation anomalies connected with the BSISO1 are unfavorable for the WPSH-SNJ in the late years.

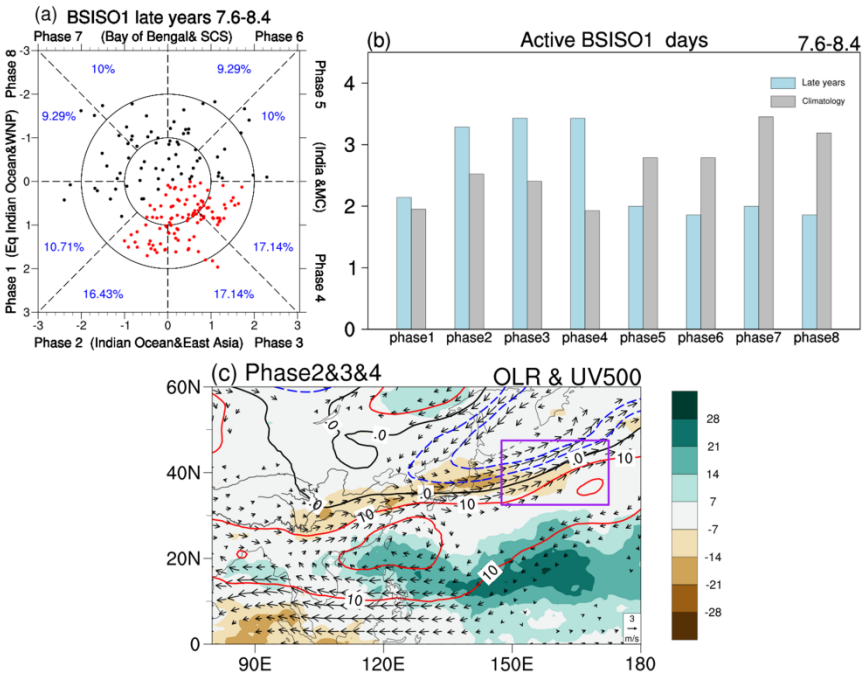

Figure 9. From July 6th pentad - August 4th pentad for late years, (a) the phase space diagram of BSISO1, the blue words represent the percentage of the days' number in each phase. (b) The active BSISO1 days in phases 1-8 (bar, unit: day), the blue and grey bars represent the active days for late years and the climatological mean, respectively. (c) The composite subseasonal anomalies of OLR (shaded, W m^{-2}), 500hPa wind (vector,m s^{-1}), and Z500 (contour, the solid red lines, and dotted blue lines indicate positive and negative values, respectively) of active BSISO1 days in Phase 2–4, the shades and vectors are shown only when they are significant at the 95% confidence level. The purple box indicates the core region of the late years.

The above results indicate that subseasonal signals in the mid-lower levels do not affect the late years. So, what factors contribute to the WPSH-SNJ in the later years? Previous studies showed that wave trains in the mid-upper levels can affect the geopotential height anomalies in the core region (Liu et al., 2019). To explore the influence of the upper-level wave train on the WPSH-SNJ, Fig. 10 shows the pentad evolution from July 6th pentad-August 4th pentad for late years, including the 300 hPa geopotential height (Z300) and horizontal wind anomalies fields. In the sixth pentad of July (Fig. 10a), a northwest-southeast tilted wave train appears over the Eurasian Continent. Propagating along the westerly jet, the wave train show a "+-+" pattern over the East European Plains, Lake Baikal, and the mid-latitude North Pacific in the first pentad of August (Fig. 10b). It results in a weak positive Z300 anomalies over the core region (green box). In the WPSH-SNJ pentad (the second pentad of August, Fig.

10c), the intensity of the wave train weakens, but the positive Z300 anomalies in the core region increase instead, which is favorable for the northward shift of the WPSH. After that, the wave train dissipates rapidly, and the positive Z300 anomalies over the core region also weaken. Consequently, we consider the eastward zonal wave train in the upper level over the Eurasian Continent as a significant factor for WPSH-SNJ in the later years.

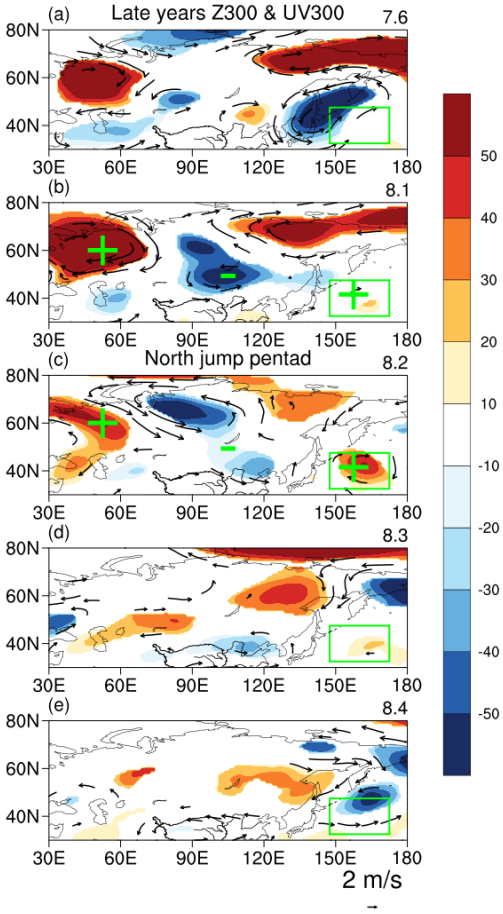

Figure 10. The composite subseasonal anomalies of geopotential height at 300 hPa (Z300) (shaded, gpm) and 300hPa horizontal wind (vector, m s^{-1}) form July 6th pentad-August 4th pentad for late years. The shading areas and vectors are shown only when they are significant at the 95% confidence level. The green boxes indicate the core region of the late years.

After exploring the influence of the upper-level wave train in the later years, we are also curious whether it acts on the WPSH-SNJ in the early years. Fig. S3 shows the anomalies in Z300 and 300 hPa horizontal wind fields from June 5th pentad - July 3rd pentad (the SNJ pentad and two pentads before and after) for

early years. Although a wave train appears over Eurasian Continent, it locates over the north side of the core region, and cannot affect the WPSH-SNJ in the early years. The enhanced Z300 anomalies over the core region during the SNJ pentad are due to the development of the positive Z500 anomalies to the upper level. Therefore, we conclude that the wave train in the upper troposphere does not play a role in the WPSH-SNJ in the early years.

Hereinbefore, we found a notable fact that although the upper-level zonal wave train weakens overall in the second pentad of August, the positive Z300 anomalies in the core region increase (Fig. 10c). It may relate to air-sea interaction (Guan et al.,2019). To explore the effect of air-sea interaction, Fig. 11 depicts the pentad evolution from July 6th pentad - August 4th pentad for late years, including the SST, turbulent flux, Z500, and 1000 hPa geopotential height (Z1000) anomalies. In the sixth pentad of July, negative Z500 anomalies are over the core region, then it turns to a weaker positive value. The positive Z500 anomalies intensify significantly in the SNJ pentad (the second pentad of August). The cold SSTAs appear in the core region in the 6th pentad of July and maintains. Affected by the sustained cold SSTAs, the negative turbulent heat flux anomaly occurs over the core area in the sixth pentad of July and continues to develop. In the second pentad of August, it significantly intensifies. As a result, weak positive Z1000 anomalies appear over the core region in the sixth pentad of July. Subsequently, the positive Z1000 anomalies gradually strengthen, enhancing markedly in the second pentad of August and maintaining until the fourth pentad of August.

To further explore the process by which SSTAs affect the geopotential height anomalies over the core region, Fig. 12 shows composite anomalies of SST, the difference between SST and 2m air temperature, latent heat flux, sensible heat flux, and Z1000 averaged over 31.5°N- 41.5°N 150°E-170°E. We also depict the spatial distribution evolution of these anomalies (Fig. S4). Since the sixth pentad of July, SSTAs consistently present negative values. Under this influence, the sea-air temperature difference gradually decreases, leading to a decrease in the sensible heat flux and latent heat flux. At the same time, a weak positive Z1000 anomaly occurs and continues to grow until the third pentad of August. It can be seen that the negative SSTAs in the core region reduce the upward sensible and latent heat fluxes, stimulating the positive Z1000 anomaly.

Fig. 12 also shows the pentad evolution of the Z300 anomalies. The Z300 anomalies have been negative from the fourth to sixth pentad of July. In the first pentad of August, due to the influence of the upper-level wave train (Fig. 10b), the Z300 anomalies turn into a positive value. This change lags behind Z1000. In the second pentad of August, accompanied by the intensification of the positive Z1000 anomalies, the positive Z300 anomalies reach the maximum and weaken rapidly.

To better represent the corresponding relationship between the upper and lower level geopotential height anomalies over the core region, Fig. 13 shows the ver-

tical profile of the geopotential height anomalies for late years averaged over 31.5°N- 41.5°N 150°E-170°E. In the first pentad of July, positive geopotential height anomalies from the upper to the lower level, showing a barotropic structure. This barotropic structure continues until the fifth pentad of July. In the sixth pentad of July, due to the influence of the cold SSTAs, the Z1000 anomaly is positive, but there are still negative anomalies in the mid-upper troposphere. A vertical baroclinic structure appears over the core region. In the first pentad of August, the Z300 anomalies turn to a positive value influenced by the wave train (Fig. 10b), and the positive Z1000 anomalies further strengthen.

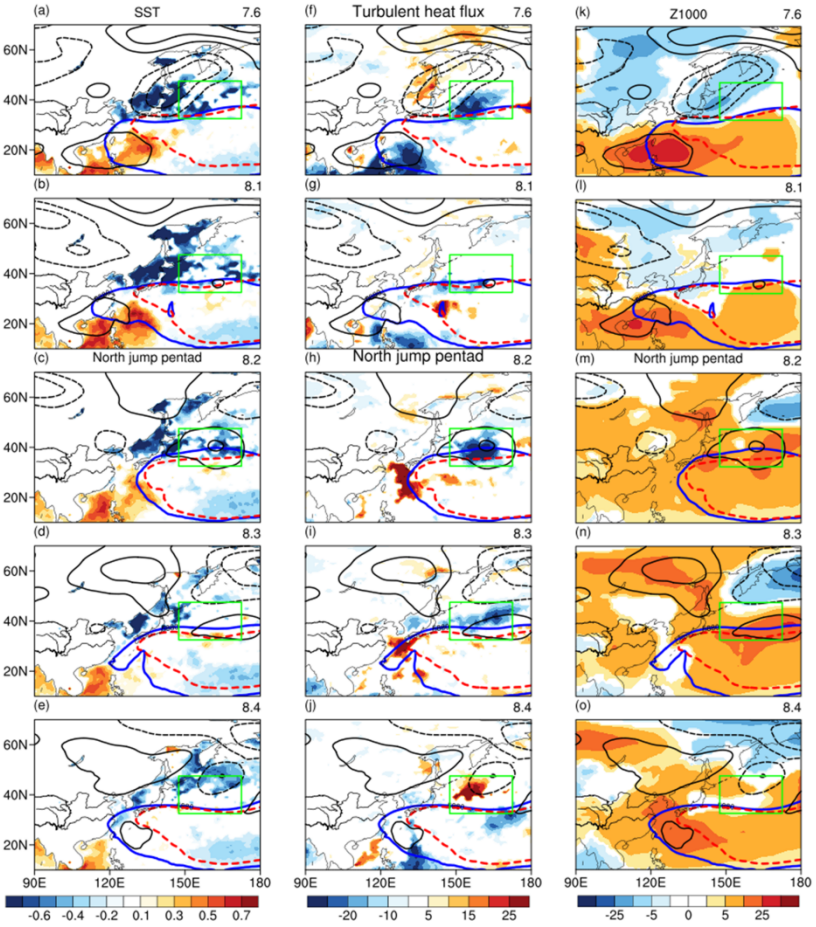

Figure 11. The composite subseasonal anomalies of (a) SSTAs (shaded, °C), (b) turbulent heat flux (shaded, positive upwards, °C). The shading areas and vectors are shown only when they are significant at the 95% confidence level. (c) The geopotential height at 1000 hPa (Z1000) (shaded, gpm) and Z500 (black contour, the solid and dotted lines indicate the positive and negative values, respectively) from July 6th pentad-August 4th pentad for late years. The shading

areas and vectors are shown only when they are statistically significant. The blue solid and red dotted lines are the 5880-lines for late years and the climatological mean, respectively. The green boxes indicate the core region of the late years.

In the SNJ pentad (the second pentad of August), the positive geopotential height anomalies of the upper and lower layers further develop. Under their interaction, the positive equivalent barotropic structure appears over the core region. After that, the positive anomaly in the upper level weakens rapidly. While the positive anomaly in the lower level continues to grow and gradually weakens after the third pentad of August.

From the above analysis, it is not difficult to find that the development of geopotential height anomalies in the upper and lower troposphere are not in-phase. The low-level positive geopotential height anomalies develop ahead of the upper-level, and they both enhance in the second pentad of August. The positive geopotential height anomalies of the entire troposphere grow significantly, contributing to the enhancement of the Z500 anomalies over the core region.

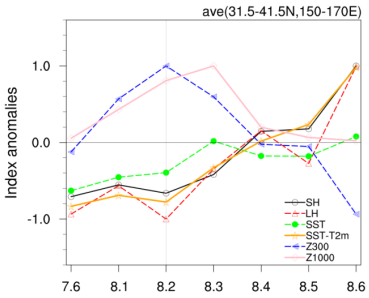

Figure 12. The composite subseasonal anomalies of SST, the difference between SST and 2m air temperature, latent heat flux, sensible heat flux, Z1000, and Z300 averaged over 31.5°N- 41.5°N for late years.

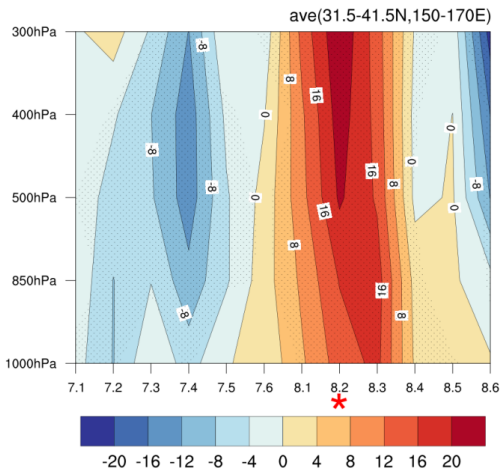

Figure 13. The vertical profile pentad evolution of the geopotential height anomalies averaged over 31.5°N- 41.5°N for late years. The red asterisk on the X axis indicates the WPSH-SNJ pentad. The dots denote statistically significant areas.

In conclusion, the characteristic of late years is that there are significant Z500 positive anomalies in the north side of the WPSH during the SNJ pentad. The region (32.5-47.5°N, 147.5-172.5°E) is defined as the core region. Different from the forcing results of the EAP pattern and BSISO in the early years, the WPSH-SNJ in the late years is affected by the east-propagating upper-level wave train and the local air-sea interaction collaboratively.

6 Summary and discussions

Based on the reanalysis datasets, this study investigates the characteristics and mechanisms of the western Pacific subtropical high (WPSH) significant northward jump during summer. According to the WPSH ridge which represents the meridional position of the WPSH (Liu et al., 2012), the WPSH significant northward jump (SNJ) events are identified from the year 1979 to 2020 during summer. It is found that the WPSH-SNJ event has critical effects on the climate of the East Asian coast. After the WPSH-SNJ, the amount of precipitation increases over Northern China, Korean Peninsula, and Indian Peninsula but decreases over Southern China, the YHR basin, and southern Japan.

The occurrence time of WPSH-SNJ events exhibits significant interannual variability. On the interannual timescale, the anomalous characteristics and different mechanisms for the early and late WPSH-SNJ years are revealed. After investigating the subseasonal evolution of the anomalous circulation characteristics, it is clearly shown that the 500 hPa geopotential height (Z500) anomalies present a "-+-" pattern over the subtropical western Pacific, Japan, and north-

east East Asia during the WPSH-SNJ pentad in the early years. The Z500 anomalies during the WPSH-SNJ pentad are found to be similar to the negative phase of the East Asia/Pacific (EAP) teleconnection pattern. Especially the core region (30-40°N, 112.5-137.5°E) in the center of the EAP tripolar geopotential height anomalies is proved to be vital for WPSH-SNJ in early years. In the SNJ early years, the EAP index shows a negative value on the sixth pentad of June. Until the first pentad of July, the positive geopotential height anomalies in the core region of the EAP pattern push the SNJ of WPSH to the north of the 28°N. The early years 500 hPa geopotential height anomalies are also related to the boreal summer intraseasonal oscillation (BSISO). The anomalous northwestward signal in BSISO1 over the Northwest Pacific Ocean can lead to the WPSH-SNJ by enhancing the positive Z500 anomalies in the core region. A total of seven earlier WPSH-SNJ events occurs from 1979 to 2020. Our work further proves that five of them are accompanied by the negative EAP index and phase 6 of BSISO1, while the remaining two events are accompanied by the positive EAP index and phase 5 of BSISO1. In general, the meridional transports of mid-lower levels tropical signals (EAP and BSISO1) are the main causes of the WPSH-SNJ in the first pentad of July, and their effects are independent on the interannual time scale.

However, in the WPSH-SNJ late years, the center of the EAP tripolar pattern shows weak negative Z500 anomalies, and the continuous positive EAP index is not conducive to the WPSH-SNJ. In addition, the active days of BSISO1 are dominant in the 2-4 phases during the later WPSH-SNJ. Although the above mid-lower levels anomalous signals are crucial to WPSH-SNJ in the early years, they have been revealed to be unrelated to the WPSH-SNJ in the late years. Our study further proves that the WPSH-SNJ in the later years is caused by the geopotential height anomalies over the region (32.5-47.5°N, 147.5-172.5°E), which is defined as another core region in WPSH-SNJ later years. The mechanisms in the SNJ late years are different from the early years. The research shows that the combined effect of the east-propagating upper-level wave train and the sea surface temperature anomalies (SSTAs) are the determinants. The continuous cold SSTAs stimulate the positive 1000 hPa geopotential height anomalies, contributing to the vertical baroclinic structure over the core region from the sixth pentad of July. On the first pentad of August, the upper-level wave train leads to the positive 300 hPa geopotential height anomalies over the core region. In the WPSH-SNJ pentad (the second pentad of August), the positive geopotential height anomalies of the upper and lower levels develop significantly. As a result, a positive anomaly with equivalent barotropic structure appears over the core region, leading to the WPSH-SNJ at this time.

This study reveals the influences of the atmospheric internal variability and external forcing on the WPSH-SNJ on the interannual timescale, including the EAP teleconnection pattern, BSISO, upper-level zonal wave train, and the SSTAs over the WNP. The meridional position of the WPSH may be also influenced by other factors, such as the atmospheric cross-equatorial flow, and thermal forcing of the Tibetan Plateau (Tao and Zhu, 1964; Xue et al., 2004;

Yang and Huang, 1989), which requires further investigation. Finally, the mechanisms of WPSH-SNJ in the anomalous early and late years are based on the fifth generation ECMWF atmospheric reanalysis dataset of the global climate (ERA-5). Further numerical simulations are needed to verify the impact factors. It is also necessary to explore the quantitative climate influences of the WPSH-SNJ with different intensities.

Acknowledgments

This work was supported by the National Key Program for Developing Basic Science (grants 2022YFE0106600), the National Natural Science Foundation of China (grants 42175060 and 42175021), the Jiangsu Province Science Foundation (Grant No. BK20201259). The authors are thankful for the support of the Jiangsu Provincial Innovation Center for Climate Change.

Open Research

The ERA-5 reanalysis data used in this study was obtained from https://www.ecmwf.int/en/forecasts/datasets/datasets/era5.

The NOAA OLR data used in this study was from https://psl.noaa.gov/data/gridded/data.olrcdr.interp.html.

The CPC precipitation data was from https://psl.noaa.gov/data/gridded/data.cpc.globalprecip.html.

References

Branstator, G. (2002). Circumglobal Teleconnections, the Jet Stream Waveguide, and the North Atlantic Oscillation. *Journal of Climate, 15*, 1893-1910. https://doi.org/10.1175/1520-0442(2002)015 <1893:CTTJSW> 2.0.CO;2

Bueh, C., Shi, N., Ji, L., Wei, J., & Tao, S. (2008). Features of the EAP events on the medium-range evolution process and the mid- and high latitude Rossby wave activities during the Meiyu period. *Chinese Science Bulletin, 53*, 610–623. https://doi.org/10.1007/s11434-008-0005-2

Chang, C. -P., Zhang, Y. S., & Li, T. (2000). Interannual and interdecadal variations of the East Asian summer monsoon and tropical Pacific SSTs. Part I: Roles of the subtropical ridge. *Journal of Climate, 13*, 4310–4325. https://doi.org/10.1175/1520-0442(2000)013<4310:iaivot>2.0.co;2

Chang, C. P., Zhang, Y., & Li, T. (2000b). Interannual and interdecadal variations of the East Asian summer monsoon and tropical Pacific SSTs. Part II: meridional structure of the monsoon. *Journal of Climate, 13*, 4326–4340. https://doi.org/10.1175/1520-0442(2000)013<4326:iaivot>2.0.co;2

Chen, G. S., & Huang, R. H. (2012). Excitation mechanisms of the teleconnection patterns affecting the July precipitation in Northwest China. *Journal of Climate, 25*,7834–7851. https://doi.org/10.1175/jcli-d-11-00684.1

Chen, Y., Song, J., & Li, C. (2016). A Study on Northward Jump of the Meiyu Rainbelt. *Chinese Journal of Atmospheric Sciences,40(4),*703-718. https://doi.org/10.3878/j.issn.1006-9895.1601.15258

Chung, P.-H., Sui, C. -H., & Li, T. (2011). Interannual relationships between the tropical sea surface temperature and summertime subtropical anticyclone over the western North Pacific. *Journal of Geophysical Research, 116*, D13111.

https://doi.org/10.1029/2010JD015554.

Ding, Y. H. (1992). Summer monsoon rainfall in China. *Journal of the Meteorological Society of Japan, 70, 373-396.*

https://doi.org/10.2151/jmsj1965.70.1B_373

Ding, Y. H., & Chan, J. C. (2005). The East Asian summer monsoon: An overview. *Meteorology;and Atmospheric Physics, 89*, 117–142.

https://doi.org/10.1007/s00703-005-0125-z

Ding, Y. H., Liu, Y. Y., & Hu, Z. Z. (2021). The Record-breaking Meiyu in 2020 and Associated Atmospheric Circulation and Tropical SST Anomalies. *Advances in Atmospheric Sciences, 38,*1980–1993.

https://doi.org/10.1007/s00376-021-0361-2

Ding, Q., & Wang, B. (2005). Circumglobal teleconnection in the Northern Hemisphere summer *Journal of Climate, 18*, 3483-3505.

https://doi.org/10.1175/JCLI3473.1

Enomoto, T., Hoskins, B. J., & Matsuda, Y. (2003). The formation mechanism of the Bonin high in August. *Quarterly Journal of the Royal Meteorological Society, 129,*157–178. https://doi.org/10.1256/qj.01.211

Guan, W. N., Hu, H. B., Ren, X. J., & Yang, X. Q. (2019). Subseasonal zonal variability of the western Pacific subtropical high in summer: climate impacts and underlying mechanisms. *Climate Dynamics, 53*, 3325-3344.

https://doi.org/10.1007/s00382-019-04705-4

He, J. H., & Liu, B. Q. (2016). The East Asian subtropical summer monsoon: Recent progress *Journal of Meteorological Research, 30(2),* 135–155.

https://doi.org/10.1007/s13351-016-5222-z

He, C., & Zhou, T. J. (2015). Decadal change of the connection between summer western North Pacific subtropical high and tropical SST in the early 1990s. *Atmospheric Science Letters, 16*, 253-259.

https://doi.org/10.1002/asl2.550

Hirota, N., & Takahashi, M. (2012). A tripolar pattern as an internal mode of the East Asian summer monsoon. *Climate Dynamics, 39*, 2219–2238. https://doi.org/10.1007/s00382-012-1416-y

Hsu, P.-C., Lee, J.-Y., & Ha, K.-J. (2016). Influence of boreal summer intraseasonal oscillation on rainfall extremes in southern China. *International Journal of Climatology, 36*, 403–1412. https://doi.org/10.1002/ joc.4433

Huang, R. H., Chen, J. L., Wang, L., & Lin, Z. D. (2012). Characteristics, processes, and causes of the spatio-temporal variabilities of the East Asian monsoon system. *Advances in Atmospheric Sciences, 29*, 910-942.

https://doi.org/10.1007/s00376-013-0001-6

Huang, S. S. (1963). A study of the longitudinal movement and its forecasting of subtropical anticyclones. *Acta Meteorologica Sinica, 33*, 320–332.

https://doi.org/10.11676/qxxb1963.030

Huang, R., & Sun, F. (1992). Impact of tropical western Pacific on the East Asian summer monsoon. *Journal of the Meteorological Society of Japan, 70*, 243-256. https://doi.org/10.2151/jmsj1965.70.1B_243

Huang, Z., Zhang, W., Geng, X., & Hsu, P. -C. (2020). Accumulated effect of intra-seasonal oscillation convections over the tropical western north pacific on the meridional location of western pacific subtropical high. *Frontiers in Earth Science, 8*, 579442. https://doi.org/10.3389/feart.2020.579442

Kikuchi, K., Wang, B., & Kajikawa, Y. (2012). Bimodal representation of the tropical Intraseasonal oscillation. *Climate Dynamics, 38*, 1989–2000. https://doi.org/10.1007/s00382-011-1159-1

Kosaka, Y., & Nakamura, H. (2010). Mechanisms of meridional teleconnection observed between a summer monsoon system and a subtropical anticyclone. Part I: The Pacific–Japan pattern. *Journal of Climate, 23*, 5085–5108.

https://doi.org/10.1175/2010JCLI3414.1.

Krishnamurthy, V., & Shukla, J. (2000). Intraseasonal and interannual variability of rainfall over India. *Journal of Climate, 13*, 4366–4377.

https://doi.org/10.1175/1520-0442(2000)0132.0.CO;2

Lee, J. Y., Wang, B., Wheeler, M. C., Fu, X., Waliser, D. E., & Kang, I. S. (2013). Real-time multivariate indices for the boreal summer intraseasonal oscillation over the Asian summer monsoon region. *Climate Dynamics, 40(1-2),* 493-509. https://doi.org/10.1007/s00382-012-1544-4

Lee, J. Y., Wang, B., Wheeler, M. C., Fu, X., Waliser, D. E., & Kang, I. S. (2017). The long-term variability of changma in the East Asian summer monsoon system: A review and revisit. *Asia-Pacific Journal of Atmospheric Sciences, 53*, 257–272. https://doi.org/10.1007/s13143-017-0032-5

Li, R., Zhou, W., & Li, T. (2014). Influences of the Pacific–Japan teleconnection pattern on synoptic-scale variability in the western north Pacific. *Journal of Climate, 27(1),* 140-154. https://doi.org/10.1175/jcli-d-13-00183.1

Liang, P., & Ding, Y. (2012). Climatologic characteristics of the intraseasonal oscillation of East Asian meiyu. *Acta Meteorologica Sinica, 70(3),* 418-435.

https://doi.org/10.11676/qxxb2012.036

Lin, H. (2013). Monitoring and predicting the intraseasonal variability of the east asian-western north pacific summer monsoon. *Monthly Weather Review, 141(3),* 1124-1138. https://doi.org/10.1175/MWR-D-12-00087.1

Liu, B. Q., Zhu, C. W., Su, J. Z., Ma, S. M., & Xu, K. (2019). Record-breaking northward shift of the western north pacific subtropical high in July 2018. *Journal of the Meteorological Society of Japan, 97*, 913—925.

https://doi.org/10.2151/jmsj.2019-047

Liu, Y. Y., Li, W. J., Ai, W. X., & Li, Q. Q. (2012). Reconstruction and application of the monthly western pacific subtropical high indices. *Journal of Applied Meteorological Science, 23*, 414-423.

https://doi.org/10.3969/j.issn.1001-7313.2012.04.004

Liu, Y. Y., Liang, P. & Sun, Y. (2019). The Asian summer monsoon: characteristics, variability, teleconnections and projection. *Cambridge*, MA: Elsevier, p237.

Lu, R. Y., Oh, J. H., & Kim, B. J. (2002). A teleconnection pattern in upper-level meridional wind over the North African and Eurasian continent in summer. *Tellus, 54*, 44–55. https://doi.org/10.1034/j.1600-0870.2002.00248.x

Madden. R. A. (1986). Seasonal-variations of the 40-50 day oscillation in the tropics. *Journal of the Atmospheric Sciences, 43,* 3138–3158. https://doi.org/10.1175/1520-0469(1986)043<3138:svotdo>2.0.co;2

Nitta, T. (1987). Convective activities in the tropical western Pacific and their impact on the northern hemisphere summer circulation. *Journal of the Meteorological Society of Japan, 65,* 373-390.

https://doi.org/10.2151/jmsj1965.65.3_373.

Qian, W. H., & J. Shi. (2017). Tripole precipitation pattern and SST variations linked with extreme zonal activities of the western Pacific subtropical high. *International Journal of Climatology, 37,* 3018–3035.

https://doi.org/10.1002/joc.4897

Ren, X. J., Yang, X. Q., & Sun, X. G. (2013). Zonal oscillation of western pacific subtropical high and subseasonal SST variations during Yangtze persistent heavy rainfall events. *Journal of Climate, 26(22),* 8929-8946.

https://doi.org/10.1175/JCLI-D-12-00861.1

Sui, C. -H., Chung, P. -H., & Li, T. (2007). Interannual and interdecadal variability of the summertime western North Pacific subtropical high. *Geophysical Research Letters, 34*, L11701.

https://doi.org/10.1029/2006GL029204.

Tao, S. Y. & Chen, L. X. (1987). A review of recent research on the East Asian summer monsoon in China. *In: Chang C-P, Krishnamurti TN (eds) Monsoon meteorology.* Oxford University Press, Oxford, pp 60–92.

Tao, S. Y. & Wei, J. (2006). The westward, northward advance of the subtropical high over the West Pacific in summer. *Journal of Applied Meteorological Science, 17*, 513−525. https://doi.org/10.3969/j.issn.1001-7313.2006.05.001.

Tao, S. Y., & Zhu, F. K. (1964). The 100-MB Flow Patterns in Southern Asia in Summer and its relation to the Advance and Retreat of the West-Pacific Subtropical Anticyclone over the Far East. *Acta Meteorologica Sinica, 4*, 387-396.

https://doi.org/10.11676/qxxb1964.039

Wang, B. & Rui, H. (1990). Synoptic climatology of transient tropical intraseasonal convection

anomalies: 1975–1985. *Meteorology and Atmospheric Physics, 44(1–4)*, 43–61. https://doi.org/10.1007/bf01026810

Wang, B. & Xie, X. (1997). A model for the boreal summer intraseasonal oscillation. *Journal of*

the Atmospheric Sciences, 54, 72–86. https://doi.org/10.1175/1520-0469(1997)054<0072:AMFTBS>2.0.CO;2

Wang, B., Wu, R. & Fu, X. (2000) Pacific-East Asian teleconnection: How does ENSO affect East Asian climate? *Journal of Climate, 13*, 1517–1536. https://doi.org/10.1175/1520-0442(2000)013<1517:PEATHD>2.0.CO;2

Wang, W., Zhou, W., Li, X., Wang, X. & Wang, D. (2016). Synoptic scale characteristics and atmospheric controls of summer heatwaves in China. *Climate Dynamics, 46*, 2923–2941. https://doi.org/10.1007/s00382-015-2741-8

Wang, Z. Y. & Ding, Y. H. (2008). Climatic Characteristics of Rainy Seasons in China. *Chinese Journal of Atmospheric Sciences, 32,* 1-13.

https://doi.org/10.3878/j.issn.1006-9895.2008.01.01

Wu, J., Xu, X. F., Jin, F. F. & Guo, P. W. (2013). Research of the intraseasonal

evolution of the East Asia Pacific pattern and the maintenance mechanism. *Acta Meteorologica Sinica, 71*, 476–491.

https://doi.org/10.11676/qxxb2013.038

Xie, S. P., Hu, K. M., Hafner, J., Tokinaga, H., Du, Y., Huang, G. & Sampe, T. (2009). Indian Ocean Capacitor Effect on Indo-Western Pacific Climate during the Summer following El Niño. *Journal of Climate, 22*, 730-747.

https://doi.org/10.1175/2008JCLI2544.1

Xie, S.P., Kosaka, Y., Du, Y., Hu, K., Chowdary, J. S. & Huang, G. (2016). Indo-western Pacific ocean capacitor and coherent climate anomalies in post-ENSO summer: A review. *Advances in Atmospheric Sciences, 33,* 411–432. https://doi.org/10.1007/s00376-015-5192-6

Xue, F., Wang, H., & He, J. H. (2004). Interannual variability of Mascarene high and Australian

high and their influences on east Asian summer monsoon. *Journal of the Meteorological Society of Japan, 82(4),* 1173-1186.

https://doi.org/10.2151/jmsj.2004.1173

Yang, H. & Sun, S. Q. (2003). Longitudinal displacement of the subtropical high in the western Pacific in summer and its influence. *Advances in Atmospheric Sciences, 20*, 921–933. https://doi.org/10.1007/BF02915515

Yang, J., Liu, Q., Xie, S. P., Liu, Z. & Wu, L. (2007). Impact of the Indian Ocean SST basin mode on the Asian summer monsoon. *Geophysical Research Letters, 34*, L02708. https://doi.org/10.1029/2006GL028571

Yang, X. Q., & Huang, S. S. (1989). The influence of intensity change of Mascarene high on the general circulation of atmosphere—A numerical experiment. *Scientia Meteorologica Sinica, 9 (2),* 125–138.

Zhang, C. D. & Dong, M. (2004). Seasonality in the Madden-Julian oscillation. *Journal of Climate, 17,* 3169–3180.

https://doi.org/10.1175/1520-0442(2004)017<3169:sitmo>2.0.co;2

Zhang, Q. Y. & Tao, S. Y. (1999). The study of the sudden northward jump of the subtropical high over the western pacific. *Acta Meteorologica Sinica, 57*, 539-548.

https://doi.org/10.1007/s00376-999-0032-1

Zhang, R., Sumi, A. & Kimoto, M. (1996). Impact of El Niño on the East Asia Monsoon: A diagnostic study of the '86/87 and '91/92 events. *Journal of the Meteorological Society of Japan, 74*, 49-62.

https://doi.org/10.2151/jmsj1965.74.1_49

Zhang, R., Sumi, A. & Kimoto, M. (1999). A diagnostic study of the impact of El Niño on the precipitation in China. *Advances in Atmospheric Sciences, 16*, 229–241. https://doi.org/10.1007/BF02973084

Zhou, T. J. & Yu, R. C. (2005). Atmospheric water vapor transport associated with typical anomalous summer rainfall patterns in China. *Journal of Geophysical Research, 110*, D08104.

https://doi.org/10.1029/2004JD005413.

Zhou, T. J., Yu, R. C., Zhang, J. & Drange, H. (2009). Why the western Pacific subtropical high has extended westward since the late 1970s? *Journal of Climate, 22*, 2199–2215. https://doi.org/10.1175/2008JCLI2527.1